Distributed Angle Estimation for Localization in Wireless Sensor Networks

Weile Zhang, Qinye Yin, Hongyang Chen, *Member, IEEE*, Feifei Gao, *Member, IEEE*, and Nirwan Ansari, *Fellow, IEEE*

***Abstract*—In this paper, we design a new distributed angle estimation method for localization in wireless sensor networks (WSNs) under multipath propagation environment. We employ a two-antenna anchor that can emit two linear chirp waves simultaneously, and propose to estimate the angle of departure (AOD) of the emitted waves at each receiving node via frequency measurement of the local received signal strength indication (RSSI) signal. An improved estimation method is further proposed where multiple parallel arrays are adopted to provide the space diversity. The proposed methods rely only on radio transceivers and do not require frequency synchronization or precise time synchronization between the transceivers. More importantly, the angle is estimated at each sensor in a completely distributed manner. The performance analysis is derived and simulations are presented to corroborate the proposed studies.**

***Index Terms*—Wireless sensor network, localization, angle of departure estimation, multipath propagation.**

I. Introduction

OWING to its highly desirable characteristic, self-localization in wireless sensor networks (WSNs) has recently attracted considerable interests [1]. Many angle-based location schemes for wireless sensor nodes have been designed and can be classified into two categories. The first category employs a rotating beam [2]–[4] generated from the anchor node at a constant angular speed, and makes use of the antenna's amplitude response. A similar technique has been developed for the conventional high-frequency direction finding systems [5]. The second category, on the other hand, makes use of the antenna's phase response. By using the multi-antenna system (MAS), the receiver is able to estimate the angle of arrival (AOA) of the wave coming from a transmitter [6], [7]. Many works in this category assumed that MAS is equipped at sensor nodes [9]. However, the hardware requirement of these schemes is substantial in large scale networks. A more acceptable choice is to equip MAS at the anchors and to let anchors estimate AOA and then feed back to the sensors [10]. However, this approach is not completely distributed, where the communication overhead and resource cost become heavy when the network density and scale increase [10].

In order to design a distributed system, several schemes targeting at angle of departure (AOD) estimation have been developed [11], [12]. The principle behind is that AOA at the MAS equipped receiver is equivalent to AOD at the MAS equipped transmitter. In [11], the anchor was designed to emit time-division pilots, by which each sensor estimated AOD in a distributed manner under perfect frequency synchronization between transceivers. Amundson *et al.* [12] proposed a radio interferometric AOD estimation method and also implemented it on a sensor network platform, where MAS with three antenna elements was equipped at the anchor. Therein, the pure sinusoidal waves were transmitted by two antennas, and the bearing of a receiver was estimated by phase measurement between the receiver and the third calibration antenna under time synchronization. Note that both [11] and [12] did not consider the multipath propagation.

In this paper, we propose a new distributed AOD estimation method for WSN localization under multipath propagation environment. We employ a two-antenna anchor that emits two linear chirp waves [8] with slight frequency difference, by which an interference field is created and the frequency of the received signal strength indication (RSSI) signal at each sensor is made relevant to the AOD information of the emitted waves. This can provide an independent AOD estimation at each sensor. In order to cope with the multipath effect, we utilize the space-alternating generalized expectation-maximization (SAGE) [13] algorithm to recursively detect the direct propagation angle, where the polynomial rooting is exploited for computational efficiency. An improved estimation method is also proposed where multiple parallel antenna arrays are adopted to provide the space diversity. In summary, the main contributions of this paper include the following.

- We introduce the chirp waves for the two-antenna interfering system to provide an independent AOD estimation at each sensor.
- We develop a polynomial rooting aided SAGE algorithm to detect the direct propagation angle with multipath

Manuscript received July 16, 2011; revised November 6, 2011, January 24 and April 20, 2012; accepted May 29, 2012. The associate editor coordinating the review of this paper and approving it for publication was S. Bahk.

This work was supported by the National Science and Technology Major Project of China under Grant No. 2010ZX03003-002-02, the National Natural Science Foundation of China under Grants No. 60971113, 61071125, 61071216, 61172093, 61172092, and 61102081, and the Science Foundation for Innovative Research Group of China under Grant No. 60921003.

W. Zhang and Q. Yin are with the Ministry of Education Key Lab for Intelligent Networks and Network Security, Xi'an Jiaotong University, Xi'an, Shaanxi, 710049, P. R. China (e-mail: wlzhang1984@gmail.com, qyyin@mail.xjtu.edu.cn).

H. Chen was with the University of Tokyo, Tokyo, Japan.

F. Gao is with Tsinghua National Laboratory for Information Science and Technology, Beijing, 100084, China, and is also with the School of Engineering and Science, Jacobs University, Bremen, 28759, Germany (e-mail: feifeigao@ieee.org).

N. Ansari is with the Advanced Networking Lab., Department of Electrical and Computer Engineering, New Jersey Institute of Technology, USA (e-mail: Nirwan.Ansari@njit.edu.).

Digital Object Identifier 10.1109/TWC.2012.121412.111346

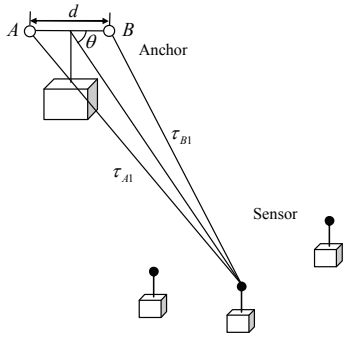

Fig. 1. Illustration of the network structure and the angle estimation. The anchor node is equipped with two antenna elements spaced by d.

propagation. We also improve the estimation performance by exploiting the space diversity from multiple parallel arrays at the anchor.

- The proposed methods are featured as distributed approaches which rely only on radio transceivers and do not require frequency synchronization or precise time synchronization between transceivers.

The rest of this paper is organized as follows. In Section II, the angle estimation method with multipath propagation is illustrated. We describe the improved method to exploit the space diversity for angle estimation in Section III. The analysis of the estimation performance and computational complexity of the proposed methods is then presented in Section IV. Simulation results are given in Section V. Finally, conclusions are drawn in Section VI.

Notations: Superscripts $(\cdot)^T$ and $(\cdot)^H$ represent transpose and Hermitian; $\Re\{\cdot\}$ and $E\{\cdot\}$ denote real part and expectation; $\mathbf{j} = \sqrt{-1}$ is the imaginary unit; diag$(\cdot)$ is a diagonal matrix with main diagonal $(\cdot)$.

II. Distributed Angle Estimation

A. System Model

Fig. 1 illustrates the sensor network consisting of three sensor nodes and one anchor node. The anchor node, equipped with two antenna elements spaced by d, is assumed to possess higher energy and longer transmission range than the sensor nodes. In the estimation stage, the anchor creates an interference field from its two antenna elements. Specifically, the elements A and B emit linear chirp waves with a common sweep slope β and a slight frequency difference; namely,

$$s_A(t) = \mathrm{e}^{\mathbf{j}(2\pi f_A t + \pi\beta t^2 + \varphi_A)}$$
$$s_B(t) = \mathrm{e}^{\mathbf{j}(2\pi f_B t + \pi\beta t^2 + \varphi_B)},$$

where f_A and f_B stand for the start sweep frequencies of elements A and B, respectively, while φ_A and φ_B denote the corresponding initial phases. Without loss of generality, $f_A > f_B$ is assumed. The constant frequency offset $f_A - f_B$ between the two emitted waves, which is rather small as compared to the radio frequency, i.e., $\left|f_A - f_B\right| \ll \frac{f_A + f_B}{2}$, is then called the sweep frequency offset (SFO). Since the two interference linear chirp waves from the two antenna elements are inspired by a common local oscillator, a dedicated SFO is guaranteed.

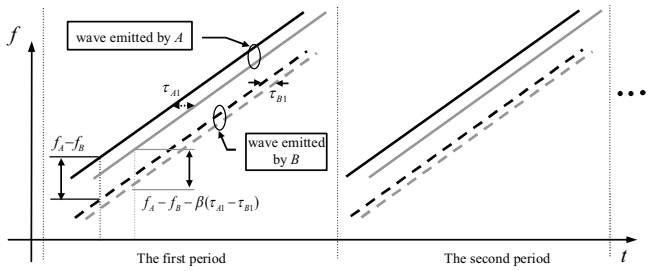

Fig. 2. Frequency versus time in the interference field. The black and gray curves represent the emitted waves at the anchor and the received waves at the sensor node, respectively.

We denote f_n and φ_n as the carrier frequency and the initial phase of the receiving sensor node, respectively. Then, in multipath environment, we model the RSSI signal as the output of an analog squarer at the receiver, with input of the down converted base-band signal, i.e.,

$$s_{rssi}(t) = \|r(t)\|^2 + w(t) \tag{1}$$

where $w(t)$ denotes the additive noise and $r(t)$ stands for the signal after down-conversion which can be expressed as

$$\begin{aligned} r(t) =& \Big(\sum\nolimits_{i=1}^{P} \alpha_{Ai} s_A(t-\tau_{Ai}) + \sum\nolimits_{j=1}^{Q} \alpha_{Bj} s_B(t-\tau_{Bj})\Big) \\ & \times \mathrm{e}^{-\mathbf{j}(2\pi f_n t + \varphi_n)} \\ =& \mathrm{e}^{-\mathbf{j}(2\pi f_n t - \pi\beta t^2 + \varphi_n)} \Big(\sum\nolimits_{i=1}^{P} \alpha_{Ai} \mathrm{e}^{\mathbf{j}(2\pi f_A t - 2\pi\beta\tau_{Ai} t + \phi_{Ai})} \\ & + \sum\nolimits_{j=1}^{Q} \alpha_{Bj} \mathrm{e}^{\mathbf{j}(2\pi f_B t - 2\pi\beta\tau_{Bj} t + \phi_{Bj})}\Big) \end{aligned} \tag{2}$$

where $\phi_{Ai} = \pi\beta\tau_{Ai}^2 - 2\pi f_A\tau_{Ai} + \varphi_A$, $\phi_{Bj} = \pi\beta\tau_{Bj}^2 - 2\pi f_B\tau_{Bj} + \varphi_B$, P and Q denote the number of multipaths from the two elements to the receiver, respectively, α_{Ai} and τ_{Ai} are the complex attenuation and propagation delay of the ith path from element A to the receiver, and α_{Bj} and τ_{Bj} are the complex attenuation and propagation delay of the jth path from element B to the receiver. Here, the multipath components are indexed so that the propagation delays are in the ascending order. Thus, τ_{A1} and τ_{B1} stand for the propagation delays of the line-of-sight (LOS) paths between the two elements and the receiver, respectively. As can be seen from (2), several different frequency shifts of the two waves are introduced at the receiver since the two waves experience different propagation delays τ_{Ai} and τ_{Bj} to the receiver. Here, similar to the assumption made in [4], [15], during the estimation process, the motion of the sensor and nearby objects is negligible, and the channel coefficients are invariant.

B. Single Path Environment as a Special Case

Let us first assume LOS paths only, i.e., $P = Q = 1$. As marked in Fig. 2, the black and gray curves represent the emitted waves at the anchor and the received waves at the sensor node, respectively. It can be seen clearly that the two sweep waves reach the receiver through different propagation delays τ_{A1} and τ_{B1}, producing a frequency shift of $-\beta(\tau_{A1} - \tau_{B1})$ at the receiving node. This frequency shift can be measured by the RSSI signal. In this situation, we

$$s_{rssi}(t) = 2|\alpha_{A1}\alpha_{B1}|\cos\Big(2\pi(f_A - f_B)t - 2\pi\beta(\tau_{A1}-\tau_{B1})t + \phi_{A1} - \phi_{B1} + \angle(\alpha_{A1}\alpha_{B1}^*)\Big) + |\alpha_{A1}|^2 + |\alpha_{B1}|^2 + w(t) \quad (3)$$

$$s_{rssi}(t) = \|\sum_{i=1}^{P}\alpha_{Ai}\mathrm{e}^{-\mathbf{j}(2\pi\beta\tau_{Ai}t-\phi_{Ai})}\|^2 + \|\sum_{j=1}^{Q}\alpha_{Bj}\mathrm{e}^{-\mathbf{j}(2\pi\beta\tau_{Bj}t-\phi_{Bj})}\|^2 + 2\Re\Big\{\sum_{i=1}^{P}\sum_{j=1}^{Q}\alpha_{Ai}\alpha_{Bj}^*\mathrm{e}^{\mathbf{j}(2\pi(f_A-f_B)t-2\pi\beta(\tau_{Ai}-\tau_{Bj})t+\phi_{Ai}-\phi_{Bj})}\Big\} + w(t). \quad (6)$$

can rewrite (1) into (3), where $\angle(\cdot)$ denotes the angle of a complex scalar. Observed from (3), the RSSI signal is a sinusoidal tone with frequency $f_A - f_B - \beta(\tau_{A1}-\tau_{B1})$. Since SFO is predetermined, the delay difference $\tau_{A1}-\tau_{B1}$ can be directly achieved through the frequency of the RSSI signal. When the distance between the transceivers is long enough, the approximation

$$\tau_{A1} - \tau_{B1} \simeq d\cos\theta/c \quad (4)$$

holds, where c denotes the speed of light and θ stands for AOD of the emitted waves from the anchor as shown in Fig. 1. The angle estimation is then immediately given by

$$\hat{\theta} = \arccos\big((\tau_{A1}-\tau_{B1})c/d\big). \quad (5)$$

Remark: In [12], the spacing between the two interfering antennas should be less than half of the radio wavelength to avoid the phase ambiguity problem. However, we use chirp waves to directly transform the delay difference to frequency offset. Thus, there is no phase ambiguity in our method, i.e., we do not have the half wavelength constraint on the antenna spacing. In fact, we will show later that increasing d improves the performance of our method.

C. Multipath Environment

With multipath propagation, the structure of RSSI is more complicated and becomes (6). The first term in (6) can be rewritten as

$$\sum_{i=1}^{P-1}\sum_{j=i+1}^{P}2|\alpha_{Ai}\alpha_{Aj}|\cos\big(2\pi\beta(\tau_{Aj}-\tau_{Ai})t+\phi_{Ai}-\phi_{Aj}+\angle(\alpha_{Ai}\alpha_{Aj}^*)\big)+\sum_{i=1}^{P}|\alpha_{Ai}|^2, \quad (7)$$

where $\tau_{Aj}-\tau_{Ai}$ stands for the propagation interval between the jth and ith paths from element A to the receiver. Note that the maximum frequency of the multiple real sinusoidal components in (7) is determined by the interval between the latest and the first paths, i.e., $\beta(\tau_{AP}-\tau_{A1})$. In other words, these frequency components will be distributed around the zero frequency in the frequency spectrum within the range of $\pm\beta(\tau_{AP}-\tau_{A1})$. Thus, to some extent, (7) illustrates the delay spread from the emitting element A to the receiver. Similar observations can be made for the second term in (6).

Furthermore, we can rewrite the last term in (6) as

$$\sum_{i=1}^{P}\sum_{j=1}^{Q}2|\alpha_{Ai}\alpha_{Bj}|\cos\big(2\pi(f_A-f_B)t-2\pi\beta(\tau_{Ai}-\tau_{Bj})t+\phi_{Ai}-\phi_{Bj}+\angle(\alpha_{Ai}\alpha_{Bj}^*)\big), \quad (8)$$

from which it is observed that at most $P\times Q$ frequency components are distributed around the SFO f_A-f_B, whereas the frequency component $f_A-f_B-\beta(\tau_{A1}-\tau_{B1})$ stands for the direct path propagation difference and can be utilized for angle estimation. Our task is to estimate $f_A-f_B-\beta(\tau_{A1}-\tau_{B1})$ while considering the other frequency components $f_A-f_B-\beta(\tau_{Ai}-\tau_{Bj})$ and the first two terms in (6) as the interferences.

It is worth mentioning that the interference from the multiple components in the first two terms becomes negligible when the spectral separation introduced by SFO f_A-f_B is set large enough. The reason will be discussed in the next subsection. In the following, we omit the influence of the first two terms and denote $L_p = P\times Q$ as the number of total frequency components. Thus, (6) can be rewritten for convenience as follows

$$s_{rssi}(t) = \sum_{l=1}^{L_p}2\cdot\alpha_l\cos\big(2\pi(f_A-f_B)t - 2\pi\beta\tau_l t + \phi_l\big) + w(t) \quad (9)$$

where $\tau_l = \tau_{Ai}-\tau_{Bj}$ denotes the time difference of the lth component, $\phi_l = \phi_{Ai}-\phi_{Bj}+\angle(\alpha_{Ai}\alpha_{Bj}^*)$, and $\alpha_l = |\alpha_{Ai}\alpha_{Bj}|$ stands for the equivalent amplitude of the lth component with $i = 1+\lfloor(l-1)/Q\rfloor$ and $j = 1+\mathrm{mod}(l-1,Q)$. The operation $\lfloor x\rfloor$ represents the integer floor.

In the conventional time of arrival (ToA) estimation, the path with minimum delay can be directly considered as the direct path, but in (9), the direct path component $\tau_{A1}-\tau_{B1}$ is concealed among the L_p components because it is neither the largest nor the smallest delay. Considering that the direct path component often possesses much stronger power, we can recognize the path with the largest power as the hidden direct path. Once the direct path is retrieved, the angle estimation can be conducted according to (5).

Remark: From the above discussion, the proposed method contains at least two advantages: 1) frequency synchronization or precise time synchronization between the transceivers is not needed;[1] 2) the angle can be estimated at each sensor in a completely distributed manner and each sensor does not need a complicated MAS.

D. DFT Analysis for RSSI Signal

Following the above discussion, our next task is to estimate the frequency of the LOS component from (9). The work in [14] provided a sophisticated method to estimate the multiple frequencies of sinusoidal components from discrete-time measurements. In our problem (9), however, we only need to estimate the LOS component, i.e., $f_A-f_B-\beta\tau_1 =$

[1]Some time synchronization among the transceivers is still required to coordinate their transmission and reception. Nevertheless, this requirement should be much more relaxed as compared to that in the conventional ToA estimation system [26].

$f_A - f_B - \beta d\cos\theta/c$. We see that the LOS component is naturally restricted within a small range of $f_A - f_B \pm \beta d/c$ with the varying scope of $2\beta d/c$. Based on this observation, we develop an efficient way to estimate the frequency of the LOS component by using discrete Fourier transform (DFT).

If we perform the DFT conversion on (9) over a period of T, the frequency resolution will be given by $\Delta f{=}1/T$, i.e., the frequency spacing between two adjacent discrete frequency spectrums. We suppose the anchor set SFO to be an integer multiple of the frequency spacing, i.e., $f_A{-}f_B{=}\upsilon\Delta f$ where υ is a predetermined integer. As mentioned earlier, this is not an unattainable task for the emitting anchor since the two linear chirp waves are inspired by a common local oscillator. Then, we need to set the antenna spacing satisfying

$$d < c/(2\beta T), \tag{10}$$

i.e., d should be set below $c/(2\beta T)$, so that the frequency varying scope of the LOS component is smaller than the frequency spacing, i.e., $2\beta d/c < \Delta f$. As a result, the main contribution of the LOS frequency component, i.e., $f_A - f_B - \beta\tau_1 = \upsilon\Delta f - \beta\tau_1$, will always be on the υth spectrum after DFT is performed. In other words, only the υth spectrum is required to be calculated for the RSSI signal. Specifically, we divide the sampled RSSI signal into K segments with N samples in each. Denoted the nth ($n{=}0,1,\cdots,N{-}1$) sample in the kth ($k = 1, 2, \cdots, K$) segment by $s_k(n)$, i.e.,

$$s_k(n) = s_{rssi}\big((k-1+n/N)\cdot T\big) + w(k,n) \tag{11}$$

where T denotes the duration of each segment, and $w(k,n){=}w((k{-}1{+}n/N){\cdot}T)$ stands for the corresponding noise item. We assume $w(k,n)$ is a real valued independent and identically distributed (i.i.d) additive white Gaussian noise (AWGN) with variance σ_n^2. We then compute the υth spectrum individually for the K segments, given by

$$Y(k) = S(k) + \tilde{w}(k) \tag{12}$$

where $\tilde{w}(k)$ has variance $N\sigma_n^2$ and is also an i.i.d random noise. Moreover,

$$\begin{aligned} S(k) &= \sum\nolimits_{n=0}^{N-1} s_k(n)\mathrm{e}^{-\mathbf{j}\frac{2\pi\upsilon n}{N}} \\ &\simeq \sum\nolimits_{l=1}^{L_p} \frac{\alpha_l \sin(\pi\beta T\tau_l)}{\sin(\pi\beta T\tau_l/N)}\mathrm{e}^{\mathbf{j}(\frac{1-N}{N}\pi\beta T\tau_l+\phi_l)}\mathrm{e}^{-\mathbf{j}2\pi(k-1)\beta T\tau_l}, \end{aligned} \tag{13}$$

where the relation $f_A{-}f_B = \upsilon/T$ is utilized and the influence from the negative frequency components due to frequency separation is omitted. Bearing in mind the first term in (6) which has been rewritten in (7), we can also compute its υth spectrum. As discussed earlier, its frequency components are distributed around the zero frequency. As a result, with large enough υ and N, its energy leakage to the υth spectrum becomes negligible. Similar observations can be found for the second term in (6).

Afterwards, for notational compactness, we can rewrite (13) as $S(k) = \sum_{l=1}^{L_p} h_l \mathrm{e}^{\mathbf{j}2\pi(k-1)\Theta_l}$, where $\Theta_l = -\beta T\tau_l$ stands for the equivalent frequency and $h_l = \delta\big(\beta T\tau_l\big)\cdot N\alpha_l\exp(\mathbf{j}(\frac{1-N}{N}\pi\beta T\tau_l+\phi_l))$ denotes its corresponding complex amplitude with $\delta(x) = \frac{\sin(\pi x)/N}{\sin(\pi x/N)}$. It is worth mentioning that the amplitudes of the components with large $|\tau_l|$ will be severely attenuated by $\delta(\beta T\tau_l)$, while the attenuation on the LOS component is rather limited due to its restriction property, i.e., $|\tau_1| < d/c$. As a result, the number of the components that have considerable influence on the υth spectrum will be much smaller than the total number of components L_p. Hence, the DFT calculation in (13) can suppress the interference, and thus improve the signal-to-interference-plus-noise ratio (SINR) for the LOS component estimation to some extent. In the next subsection, we will design a way to estimate Θ_1 associated with the direct path component. Once the estimation is done, the angle can be obtained from $\hat{\theta} = \arccos\left(-\frac{c}{\beta T d}\hat{\Theta}_1\right)$.

Remark: Define $\tau_d = \max(\tau_{AP},\tau_{BQ}) - \min(\tau_{A1},\tau_{B1})$, which represents the delay spread of the channels between the two antenna elements and the receiver. Then, to suppress the interference from the frequency components around the zero frequency, the SFO should satisfy $f_A - f_B = \upsilon/T \gg \beta\tau_d$, i.e., $\upsilon \gg \beta T\tau_d$. Note that the omitted negative frequency components in (13) can be expressed as

$$\sum_{l=1}^{L_p} \frac{\alpha_l \sin(\pi(2\upsilon-\beta T\tau_l))}{\sin(\pi(2\upsilon-\beta T\tau_l)/N)}\mathrm{e}^{\mathbf{j}(\frac{1-N}{N}\pi(2\upsilon-\beta T\tau_l)-\phi_l)}\mathrm{e}^{\mathbf{j}2\pi(k-1)\beta T\tau_l}. \tag{14}$$

Hence, $2\upsilon - \beta T\tau_l \le 2\upsilon + \beta T\tau_d \ll N$ is also required to support the approximation of (13). Then, we arrive at $\beta T\tau_d \ll \upsilon \ll \frac{N-\beta T\tau_d}{2}$. Bearing in mind that $T = N/F_s$ with F_s being the sampling rate at the receiver, we further obtain

$$\beta\tau_d \ll \frac{\upsilon}{N}F_s \ll \frac{F_s - \beta\tau_d}{2}. \tag{15}$$

Hence, when $\frac{F_s-\beta\tau_d}{2} \gg \beta\tau_d$, υ can be set based on the criterion of (15). This also indicates $F_s \gg 3\beta\tau_d$, i.e., the sampling rate at the receiver should be much larger than the value of $3\beta\tau_d$.

E. Estimation Algorithm

Let us first consider the special case when only the LOS paths exist. In this case, RSSI will be a sine wave and we stack the K spectrums as

$$\mathbf{Y} = \big[Y(1), Y(2), \cdots, Y(K)\big]^T = h_1\boldsymbol{a}(\Theta_1) + \tilde{\mathbf{w}} \tag{16}$$

where $\boldsymbol{a}(\Theta_1) = [1, \mathrm{e}^{\mathbf{j}2\pi\Theta_1}, \cdots, \mathrm{e}^{\mathbf{j}2\pi(K-1)\Theta_1}]^T$ is a Vandermonde vector and $\tilde{\mathbf{w}}$ is the corresponding AWGN vector. The maximum likelihood (ML) estimation of Θ_1 is given by

$$\hat{\Theta}_1 = \arg\max_{\Theta} g(\Theta), \tag{17}$$

where $g(\Theta) = \boldsymbol{a}(\Theta)^H\mathbf{Y}\mathbf{Y}^H\boldsymbol{a}(\Theta)$. An important observation here is that the maximization problem of (17) can be implemented by polynomial rooting with high computational efficiency. The basic idea is first obtaining all local minimum/maximum solutions by setting the derivative of the cost function to be zero, and then putting these solutions back to the original cost function and selecting the maximum after comparisons [19]. Specifically, we obtain $\frac{\partial g(\Theta)}{\partial\Theta} = \boldsymbol{a}(\Theta)^H\big(\mathbf{\Phi}\mathbf{Y}\mathbf{Y}^H - \mathbf{Y}\mathbf{Y}^H\mathbf{\Phi}\big)\boldsymbol{a}(\Theta)$ where $\mathbf{\Phi} = \mathbf{j}2\pi\mathrm{diag}\big(0,\cdots,K{-}1\big)$. Then, according to [19], we know $z = \mathrm{e}^{\mathbf{j}2\pi\hat{\Theta}_1}$ is one of the roots for the polynomial $Q(z) = \sum_{k=-K+1}^{K-1} a_k z^k$ where

$$a_k = \sum\nolimits_{q-p=k}[\mathbf{T}]_{pq} \quad \text{and} \quad \mathbf{T} = \mathbf{\Phi}\mathbf{Y}\mathbf{Y}^H - \mathbf{Y}\mathbf{Y}^H\mathbf{\Phi}. \tag{18}$$

By putting the roots on the unit circle of $Q(z)$ back to the original cost function $g(\Theta)$ and selecting the maximum after comparisons, the solution to (17) is obtained.

For the general multipath case, there exist two estimation techniques, i.e., the SAGE algorithm [13] and the subspace-based approaches, such as root multiple signal classification (MUSIC) [15] and estimation via rotational invariance techniques (ESPRIT) [16]. In this paper, we focus only on the SAGE method since the subspace based methods are sometimes less robust [17]. The SAGE algorithm iteratively estimates $\{h_l, \Theta_l\}_{l=1}^{L_p}$ by maximizing the following likelihood function $L\big(\{h_l, \Theta_l\}_{l=1}^{L_p}\big) = -\sum_{k=1}^{K}\big(Y(k) - S(k)\big)^2$. Similar to the expectation-maximization (EM) algorithm [18], the iteration of SAGE consists of two steps, i.e., the expectation (E-step) and the maximization (M-step). Each iteration consists of L_p cycles, and the parameters are updated sequentially within each iteration.

Specifically, the $(n+1)$th iteration of the SAGE algorithm consists of the following steps.

For $l = 1, 2, \cdots, L_p$,

E-step: Estimate the "complete" data for the lth path

$$\hat{X}_l^{(n)}(k) = Y(k) - \sum_{i=1}^{l-1} \hat{h}_i^{(n+1)} \mathrm{e}^{\mathrm{j}2\pi(k-1)\hat{\Theta}_i^{(n+1)}} - \sum_{i=l+1}^{L_p} \hat{h}_i^{(n)} \mathrm{e}^{\mathrm{j}2\pi(k-1)\hat{\Theta}_i^{(n)}}, \tag{19}$$

where $\hat{h}_l^{(n)}$ and $\hat{\Theta}_l^{(n)}$ are the estimations of h_l and Θ_l in the nth iteration, respectively.

M-step: Update the delay and amplitude of the lth path

$$\hat{\Theta}_l^{(n+1)} = \arg\ \max_{\Theta} |\zeta_l^{(n)}(\Theta)|^2, \quad \hat{h}_l^{(n+1)} = \zeta_l^{(n)}(\hat{\Theta}_l^{(n+1)})/K \tag{20}$$

where $\zeta_l^{(n)}(\Theta) = \sum_{k=1}^{K} \hat{X}_l^{(n)}(k)\mathrm{e}^{-\mathrm{j}2\pi(k-1)\Theta}$. By denoting $\hat{\mathbf{X}}_l^{(n)} = \big[X_l^{(n)}(1), X_l^{(n)}(2), \cdots, X_l^{(n)}(K)\big]^T$, we have $|\zeta_l^{(n)}(\Theta)|^2 = \boldsymbol{a}(\Theta)^H \hat{\mathbf{X}}_l^{(n)} (\hat{\mathbf{X}}_l^{(n)})^H \boldsymbol{a}(\Theta)$. Thus, the polynomial rooting approach in (17)-(18) can be adopted in (20) more efficiently.

The SAGE algorithm can be initialized with the pre-initial setting of all zeros, i.e., $\hat{\Theta}_l^{(0)} = 0$, $(l = 1, 2, \cdots, L_p)$. Such a technique is commonly referred to as successive interference cancelation [13]. The first component picked out in the initialization often has the most dominant power indication. Thus, after convergence, the output of $\hat{\Theta}_1^{(n+1)}$ can be considered as the direct path.

Remark: As pointed out earlier, the number of components that have considerable influence on the expected spectrum will be much smaller than $P \times Q$. Thus, in practice, the parameter L_p in the above SAGE algorithm can be set as a value large enough to capture all the dominant components while it is at the same time significantly smaller than $P \times Q$.

III. Improved Estimation with Space Diversity

Owing to the randomness of the wireless multipath channel, the correct angle may not be obtained even in the absence of noise, thus producing the well-known non-line-of-sight (NLOS) errors, for example, when the LOS path is obstructed or when the LOS measurements are contaminated by the reflected and/or diffracted signals. Several techniques to mitigate the NLOS error in angle-based localization have been investigated, see for example [20].

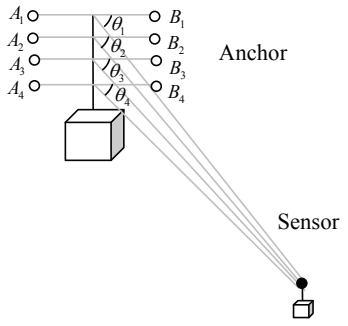

Fig. 3. Illustration of the improved angle estimation with space diversity. The AODs between the multiple parallel arrays and the receiving sensor, i.e., θ_m, $m = 1, 2, \cdots, 4$, can be considered the same.

Different from these mitigation approaches, in order to suppress the NLOS errors, we deploy multiple antenna arrays at the emitting anchor to exploit the diversity benefit. The key observation is that AODs between multiple parallel arrays and the receiving sensor can be considered the same. An example is given in Fig. 3, where $\theta_1 \simeq \theta_2 \simeq \theta_3 \simeq \theta_4$ holds from the geometry relation, with θ_m standing for AOD between the mth array and the receiver. In the following, we denote M as the number of the arrays equipped at the anchor, and approximate that the M AODs θ_m $(m = 1, 2, \cdots, M)$ are identical and can be denoted by a single AOD θ. By simple analysis, this approximation error can be neglected when the anchor-sensor distance is large enough. Then, if the spacing between the adjacent arrays is larger than the coherence distance, the channels between different arrays and the receiver can be considered independent. Our basic idea is that, although it is possible that some LOS path is obstructed or contaminated, the possibility of the LOS paths from M arrays to be all obstructed or contaminated will be significantly much smaller. Based on this observation, we then exploit diversity to greatly suppress the NLOS errors.

Without loss of generality, we assume the channel lengths between the two elements A_m and B_m in the mth array and the receiver are all equal to P and Q, respectively. Their channel components are correspondingly denoted by $\{\tau_{Ai,m}, \alpha_{Ai,m}\}_{i=1}^{P}$ and $\{\tau_{Bj,m}, \alpha_{Bj,m}\}_{j=1}^{Q}$. Besides, we let the element spacing in each array equals d, and the direct time differences $\tau_{A1,m} - \tau_{B1,m} = d\cos\theta$ $(m = 1, 2, \cdots, M)$ are then identical. In the estimation process, each array in the anchor emits the interference linear chirp waves sequentially. During the period when the mth array is emitting, the received RSSI signal at the sensor node is

$$s_{rssi,m}(t) = \sum_{l=1}^{L_p} 2\alpha_{l,m} \cos\big(2\pi(f_A - f_B)t - 2\pi\beta\tau_{l,m}t + \phi_{l,m}\big) + w_m(t) \tag{21}$$

where $\alpha_{l,m} = |\alpha_{Ai,m}\alpha_{Bj,m}|$, $\tau_{l,m} = \tau_{Ai,m} - \tau_{Bj,m}$ and $\phi_{l,m} = \phi_{Ai,m} - \phi_{Bj,m} + \angle(\alpha_{Ai,m}\alpha_{Bj,m}^*)$ with $i = 1 + \lfloor (l-1)/Q \rfloor$ and $j = 1 + \mathrm{mod}(l-1, Q)$. Similar to (12), the vth

spectrum of (21) can be expressed as

$$Y_m(k) = \sum_{l=1}^{L_p} h_{l,m} \mathrm{e}^{\mathbf{j}2\pi(k-1)\Theta_{l,m}} + \tilde{w}_m(k), \tag{22}$$

where $\Theta_{l,m} = -\beta T \tau_{l,m}$, $h_{l,m} = N\alpha_{l,m} \exp(\mathbf{j}(\frac{N-1}{N}\beta T \tau_{l,m} + \phi_{l,m})) \cdot \delta\big(\beta T \tau_{l,m}\big)$ and $\tilde{w}_m(k)$ is the corresponding AWGN item with variance $N\sigma_n^2$.

We first consider the case when only the LOS paths exist. Stacking the K spectrums gives

$$\begin{aligned}\mathbf{Y}_m =& \big[Y_m(1), Y_m(2), \cdots, Y_m(K)\big]^T \\ =& h_{1,m}\boldsymbol{a}(\Theta_{1,m}) + \tilde{\mathbf{w}}_m\end{aligned} \tag{23}$$

where $\tilde{\mathbf{w}}_m$ is the corresponding AWGN vector. Since $\Theta_{1,m}$ will be identical for different arrays m, we denote $\Theta_1 = \Theta_{1,m}$, $(m = 1, 2, \cdots, M)$. Then, the snapshot matrix for estimation can be obtained as:

$$\mathbf{Y} = \big[\mathbf{Y}_1, \mathbf{Y}_2, \cdots, \mathbf{Y}_M\big] = \mathbf{h}_1 \boldsymbol{a}(\Theta_1) + \tilde{\mathbf{W}} \tag{24}$$

where $\mathbf{h}_1 = [h_{1,1}, h_{1,2}, \cdots, h_{1,M}]$ and the corresponding AWGN matrix is denoted by $\tilde{\mathbf{W}} = [\tilde{\mathbf{w}}_1, \tilde{\mathbf{w}}_2, \cdots, \tilde{\mathbf{w}}_M]$. In this case, the polynomial rooting in (17)-(18) can also be adopted to estimate Θ_1 in the ML sense.

Next, we consider the general case of multipaths. If we denote the "complete" data in the nth iteration for the lth component of the received signal from the mth array by $\hat{X}_{l,m}^{(n)}$, then the estimation for the direct component in the $(n+1)$th iteration can be updated as

$$\hat{\Theta}_{1,m}^{(n+1)} = \arg\max_{\Theta} \sum_{m=1}^{M} |\zeta_{1,m}^{(n)}(\Theta)|^2, \tag{25}$$

$m = 1, 2, \cdots, M$, where $\zeta_{l,m}^{(n)}(\Theta) = \sum_{k=1}^{K} \hat{X}_{l,m}^{(n)} \mathrm{e}^{-\mathbf{j}2\pi(k-1)\Theta}$ denotes the corresponding cost function. We can describe the $(n+1)$th iteration of the improved algorithm as follows:

For $l = 1, 2, \cdots, L_p$,

E-step: Estimate the "complete" data for the lth path from M arrays separately.

For $m = 1, 2, \cdots, M$,

$$\begin{aligned}\hat{X}_{l,m}^{(n)}(k) =& Y_m(k) - \sum_{i=1}^{l-1} \hat{h}_{i,m}^{(n+1)} \mathrm{e}^{\mathbf{j}2\pi(k-1)\hat{\Theta}_{i,m}^{(n+1)}} \\ & - \sum_{i=l+1}^{L_p} \hat{h}_{i,m}^{(n)} \mathrm{e}^{\mathbf{j}2\pi(k-1)\hat{\Theta}_{i,m}^{(n)}},\end{aligned} \tag{26}$$

where $\hat{h}_{l,m}^{(n)}$ and $\hat{\Theta}_{l,m}^{(n)}$ are the estimations of $h_{l,m}$ and $\Theta_{l,m}$ in the nth iteration, respectively.

M-step:

(1) Update the delay of the lth path:

If $l = 1$, i.e., the direct component, update the delay by using (25).

If $l \neq 1$, update the delay from M arrays separately:

For $m = 1, 2, \cdots, M$,

$$\hat{\Theta}_{l,m}^{(n+1)} = \arg \max_{\Theta} |\zeta_{l,m}^{(n)}(\Theta)|^2. \tag{27}$$

(2) Update the amplitude of the lth component from M arrays separately:

For $m = 1, 2, \cdots, M$,

$$\hat{h}_{l,m}^{(n+1)} = \zeta_{l,m}^{(n)}\big(\hat{\Theta}_{l,m}^{(n+1)}\big)/K. \tag{28}$$

Note that the solutions of (25) and (27) can also be derived by using polynomial rooting more efficiently as (20).

IV. Performance Analysis

A. Estimation Performance

In this subsection, we analyze the angle estimation performance of our methods for the special case of considering only the LOS paths. For comparison, the methods without and with space diversity are referred to as Basic Angle Estimation (BAE) and Improved Estimation with Space Diversity (IESD), respectively. Also, for fairness, we assume that the sweeping process in BAE is repeated M times and the sensor utilizes M snapshots to estimate the angle.

From (16), we know that BAE is equivalent to estimate the single frequency from the observed K complex samples. The Cramer-Rao lower bound (CRLB) of the frequency estimation variance for (16) can be computed as $\sigma_{\Theta_1}^2 = \Big(\frac{1}{2\pi}\Big)^2 \frac{6N}{MK(K^2-1)|h_1|^2} \cdot \frac{1}{\rho}$ where $\rho = 1/\sigma_n^2$ stands for the system signal-to-noise ratio (SNR) and $|h_1| = \delta\big(\frac{\beta T d \cos\theta}{c}\big) \cdot N\alpha_1$ [21]. Let us denote $\gamma = |\alpha_1|^2$ and ignore the approximation errors in (4) and (13), and then CRLB of the angle estimation is given by

$$\sigma_\theta^2 = \Big(\frac{c}{\beta T d \sin\theta}\Big)^2 \cdot \sigma_{\Theta_1}^2 = \frac{\epsilon^2}{\gamma} \tag{29}$$

where $\epsilon = \big(\frac{c}{2\pi\beta T d \delta\big(\frac{\beta T d \cos\theta}{c}\big)\sin\theta}\big)\sqrt{\frac{6}{\rho MK(K^2-1)N}}$. Note that the approximation error in (4) will bring a slight estimation bias. Also, a trivial noise enhancement will be introduced by the approximation error in (13). However, we still adopt (29) as a benchmark to evaluate the performance for simplicity. Similarly, CRLB of the angle estimation for IESD can be expressed as

$$\tilde{\sigma}_\theta^2 = \frac{M \cdot \epsilon^2}{\tilde{\gamma}} \tag{30}$$

where $\tilde{\gamma} = \sum_{m=1}^{M} |\alpha_{1,m}|^2$. Note that with a large N, we know $\delta(x) \simeq \frac{\sin \pi x}{\pi x}$ and then $\epsilon \simeq \frac{c \cdot \cot\theta}{2\sin(\pi\beta T d \cos\theta)}\sqrt{\frac{6}{\rho MK(K^2-1)N}}$. For any given realizations of γ and $\tilde{\gamma}$, we see that both σ_θ^2 and $\tilde{\sigma}_\theta^2$ can be decreased by increasing d when d is within the maximum value from (10), implying that a larger antenna spacing d can improve the performance of our methods.[2]

Next, we assume $|\alpha_1|$ and $|\alpha_{1,m}|$ obey Rayleigh distribution with unit parameter. Then, γ obeys an exponential distribution while $\tilde{\gamma}$ follows a Gamma distribution. Their probability density function (PDF) can be expressed as

$$f_\gamma(y) = \mathrm{e}^{-y}, \quad f_{\tilde{\gamma}}(y) = \frac{y^{M-1}\mathrm{e}^{-y}}{(M-1)!}, \tag{31}$$

respectively. Averaging the above CRLBs over the random channels yields

$$\int_0^\infty \sigma_\theta^2 \cdot f_\gamma(y) dy = \infty, \tag{32}$$

$$\int_0^\infty \sigma_{\tilde{\theta}}^2 \cdot f_{\tilde{\gamma}}(y) dy = \frac{M}{M-1}\epsilon^2 = \frac{6\varsigma^2}{(M-1)K(K^2-1)N\rho}, \tag{33}$$

[2]Strictly speaking, the approximation error of (4) increases with d. Nonetheless, this approximation error can be neglected in large scale networks.

where $\varsigma=\frac{c}{2\pi\beta T d\delta\left(\frac{\beta T d\cos\theta}{c}\right)\sin\theta}$. The comparison between (32) and (33) illustrates the superiority of IESD to some extent. Practically, the angle estimation error will also be restricted within π and the estimation variance of BAE cannot become infinite.

In the following, we assume that the angle estimation errors obey the Gaussian distribution, which is also a valid assumption proved in [22]; that is, the estimation error of the ESPRIT algorithm with enough snapshots, which approaches CRLB performance, will obey the Gaussian distribution. When the absolute angle estimation error is larger than a threshold ϕ, we claim the estimation fails or there is a NLOS error. Then, the estimation failure probability (EFP) of IESD can be computed from

$$\tilde{P}_{EFP}=2\cdot\int_0^\infty\Big(\int_\phi^\infty\frac{1}{\sqrt{2\pi}\sigma_{\tilde{\theta}}}\mathrm{e}^{-\frac{x^2}{2\sigma_{\tilde{\theta}}^2}}dx\Big)f_{\tilde{\gamma}}(y)dy. \quad (34)$$

Substituting (30) and (31) into (34) gives

$$\tilde{P}_{EFP}=\frac{2\Gamma(M+\frac{1}{2})}{\sqrt{2\pi M}\epsilon(M-1)!}\int_\phi^\infty\frac{1}{(1+\frac{x^2}{2L\epsilon^2})^{M+\frac{1}{2}}}dx \quad (35)$$

where $\Gamma(\cdot)$ stands for the Gamma function. Using the equation [23, eq. (2.271.6)], the closed form for EFP of IESD can be expressed as

$$\tilde{P}_{EFP}=\sum_{k=0}^{M-1}\frac{(-1)^k2\Gamma(M+\frac{1}{2})}{\sqrt{\pi}(2k+1)k!(M-k-1)!}\times\Big(1-\frac{\phi^{2k+1}}{(2M\epsilon^2+\phi^2)^{\frac{2k+1}{2}}}\Big). \quad (36)$$

At high SNR region, (35) can be rewritten as

$$\begin{aligned}\tilde{P}_{EFP}=&\frac{2^{M+1}\Gamma(M+\frac{1}{2})}{\sqrt{\pi M}\epsilon(M-1)!}\int_\phi^\infty\frac{M^{\frac{2M+1}{2}}\epsilon^{2M+1}}{x^{2M+1}}dx+\mathcal{O}(\epsilon^{2M})\\=&\frac{\varsigma^{2M}6^M(2M-1)!!}{\phi^{2M}M!K^M(K^2-1)^MN^M}\frac{1}{\rho^M}+\mathcal{O}(\frac{1}{\rho^M}). \quad (37)\end{aligned}$$

where $\mathcal{O}(\cdot)$ is a higher order infinitesimal of $(\cdot)$, and $(2M-1)!!$ stands for the double factorial notation. From (37), we observe that the diversity gain of the detection is M.

Likewise, the closed form for EFP of BAE can be denoted as

$$\begin{aligned}P_{EFP}=&2\cdot\int_0^\infty\Big(\int_\phi^\infty\frac{1}{\sqrt{2\pi}\sigma_\theta}\mathrm{e}^{-\frac{x^2}{2\sigma_\theta^2}}dx\Big)f_\gamma(y)dy\\=&1-\frac{\phi}{\sqrt{2\epsilon^2+\phi^2}}. \quad (38)\end{aligned}$$

In the high SNR region, it becomes $P_{EFP}=\varsigma^2\cdot\frac{6}{\phi^2MK(K^2-1)N}\cdot\frac{1}{\rho}+\mathcal{O}(\frac{1}{\rho})$. Then, we have

$$\frac{\tilde{P}_{EFP}}{P_{EFP}}\simeq\Big(\frac{6\varsigma^2}{\phi^2K(K^2-1)N}\Big)^{M-1}\frac{(2M-1)!!}{(M-1)!}\cdot\frac{1}{\rho^{M-1}}. \quad (39)$$

From (39), we know that as the SNR increases, the ratio in (39) will be declined exponentially with parameter $M-1$, implying that the gap between BAE and IESD will be dramatically increased.

B. Computational Complexity Analysis

We provide a brief analysis on the computational complexity of our methods in terms of the number of complex multiplications (CMs). Note that to derive $\hat{\Theta}_{l,m}^{(n+1)}$, a polynomial rooting with the highest order of $2K-2$ is needed whose complexity is equivalent to calculating the eigenvalues of a $(2K-2)\times(2K-2)$ matrix. From [24], we know its complexity is approximately given by $10(2K-2)^3$ if the QR algorithm is adopted for eigenvalues calculation. In Table I, we list the required CMs for calculating the different items of IESD,[3] where L_c denotes the number of iterations. For the most complicated case in our simulations, i.e., $N=256$, $K=16$, $M=8$, $L_c=2$ and $L_p=4$, the total complexity is around 1.39×10^7 CMs.

V. Simulations

In the simulations, the radio frequency is $(f_A+f_B)/2=2.45$ GHz. Considering a typical delay spread $\tau_d=1$ μs [25] and the largest sweep slope adopted later in our simulations $\beta=1.6$ MHz/1 ms, the sampling rate at the sensor node has to satisfy $F_s\gg4.8$ KHz. In our simulations, we set $F_s=40$ KHz and $N=256$. We further set $\upsilon=64$ to satisfy the condition of (15), which is also verified later to be able to suppress the unexpected interference. The duration of one segment is then $T=6.4$ ms. The antenna spacing d is set below the right hand side of (10).

A. Scenarios with only the LOS Path

First, we consider only the LOS paths between the transceivers. In the simulations, the sensor nodes are randomly distributed in the sector area with AOD varied from $\pi/6$ to $5\pi/6$ and distance between the anchor from 20 m to 200 m. We assume the amplitude of $|\alpha_1|$ and $|\alpha_{1,m}|$ obey the same Rayleigh distribution with unit parameter. We compare the angle estimation performance between BAE and IESD, where four arrays are adopted in the latter, i.e., $M=4$. For fairness, the sweeping process is repeated four times in BAE. We set $K=8$ and $d=5$ m unless otherwise specified. Besides, for comparison, we modify [12] by adopting the high precise frequency domain phase measurement. We refer to [12] as PDM, as it relies on the phase difference measurement between the transceivers. Specifically, we assume in PDM, the frequency difference between the two emitted sinusoidal waves is the same as ours, i.e., $\upsilon/T=10$ KHz. For fairness, we assume the receiving node collects samples with the same sampling rate and duration as ours, and then calculates the phase of corresponding spectrum with a total of MKN samples. Moreover, phase measurement under perfect time synchronization is assumed in PDM, and we consider the calibration antenna has the knowledge of its perfect phase measurement.

We vary the sweep slope from $\beta=0.8\,\mathrm{MHz}/1\,\mathrm{ms}$ to $\beta=1.6\,\mathrm{MHz}/1\,\mathrm{ms}$; thus, the sweep bandwidth increases from 40.96 MHz to 81.92 MHz. The angle estimation root mean square error (RMSE) versus the SNR is shown in Fig. 4 under

[3]The results of $M=1$ correspond to the computational complexity of BAE.

TABLE I
COMPUTATIONAL COMPLEXITY ANALYSIS OF OUR METHOD (IESD).

Calculation items	CMs
$Y_m(k), k=1,\cdots,K, m=1,\cdots,M$	KMN
$\hat{X}_{l,m}^{(n)}(k), k=1,\cdots,K,$ $l=1,\cdots,L_p, m=1,\cdots,M, n=0,\cdots,L_c$	$L_pKM(1+L_c)(L_p-1)$
$\hat{\Theta}_{1,m}^{(n+1)}, m=1,\cdots,M, n=0,\cdots,L_c$	$(1+L_c)(3MK^2/2+10(2K-2)^3+2MK(2K-2))$
$\hat{\Theta}_{l,m}^{(n+1)}, l=2,\cdots,L_p,$ $m=1,\cdots,M, n=0,\cdots,L_c-1$	$ML_c(L_p-1)(3K^2/2+10(2K-2)^3+2K(2K-2))$
$\hat{h}_{l,m}^{(n+1)}, m=1,\cdots,M,$ $l=1,\cdots,L_p, n=0,\cdots,L_c-1$	$ML_pL_c(K+1)$

several scenarios. The results are obtained by averaging 10^5 independent trials. We make the following three observations.

First, the simulation results illustrate the performance superiority of IESD and the performance improvement with the larger sweep bandwidth. We also show the performance of BAE under non-attenuation environment by the dotted curve,[4] i.e., $|\alpha_1| = 1$. We see that with BAE, there is a large gap between the attenuation and non-attenuation environment. However, attributed to the exploited diversity, IESD with four arrays almost approaches this non-attenuation performance. Moreover, the analyzed CRLB results computed by averaging (33) over AOD from $\pi/6$ to $5\pi/6$ are also presented by the dashed curves. It is shown that with the polynomial rooting approach, the simulation results have closely approached the CRLB curves. Here, we should note that IESD can work under the low SNR condition, e.g., -10 dB. This benefits from the SNR gain introduced by the calculation of the N-point DFT spectrum in (12). Note that in (9), the power of the direct path component and the noise is $2|\alpha_1|^2$ and σ_n^2, respectively. After the DFT calculation, from (12) and (13), we know the power of the direct path component and the noise become $|\alpha_1|^2\frac{\sin^2(\pi\beta T\tau_1)}{\sin^2(\pi\beta T\tau_1/N)} \simeq N^2|\alpha_1|^2\frac{\sin^2(\pi\beta T\tau_1)}{(\pi\beta T\tau_1)^2}$ and $N\sigma_n^2$, respectively. Thus, the SNR gain, i.e., the ratio of the power gains between the direct path component and the noise, is $\rho_{gain} = 10\log_{10}(\frac{N\sin^2(\pi\beta T\tau_1)}{2(\pi\beta T\tau_1)^2})$. It can be easily verified $\rho_{gain} > 19.78$ dB in our example.

Second, we see that with the high precise frequency domain phase measurement, the PDM also achieves a satisfactory performance under perfect time synchronization. However, our approach can behave better with a large enough sweep bandwidth; moreover, we do not rely on any precise time synchronous measurement between the transceivers.

Third, we increase the antenna spacing from 5 m to 10 m and show the results in Fig. 4.[5] As expected, we see that IESD obtains better performance with a larger antenna spacing. Moreover, we also observe a slight error floor appears under the relative higher SNR region due to the approximation error in (4).

The corresponding EFP performance is depicted in Fig. 5, where CRLB analysis results computed by averaging (38) and (36) over AOD from $\pi/6$ to $5\pi/6$ are also presented by the dashed curves. We set the threshold for the angle estimation error $\phi = 2\pi/180$ in this example. The number of independent trials is adapted in order to guarantee that at least 100 estimation failures are achieved. The simulation results confirm our analysis and the curves closely match the analytical results derived from CRLB. The results also verify the superiority of IESD. Especially, the performance improvement derived from the space diversity can be observed from the slope of curves, and is in correspondence with our diversity analysis. We see that BAE requires SNR larger than 5 dB to obtain EFP below 1%, whereas less than 0 dB is needed in IESD. It is also observed that since diversity is not exploited in PDM, its slope is significantly smaller than that of IESD.

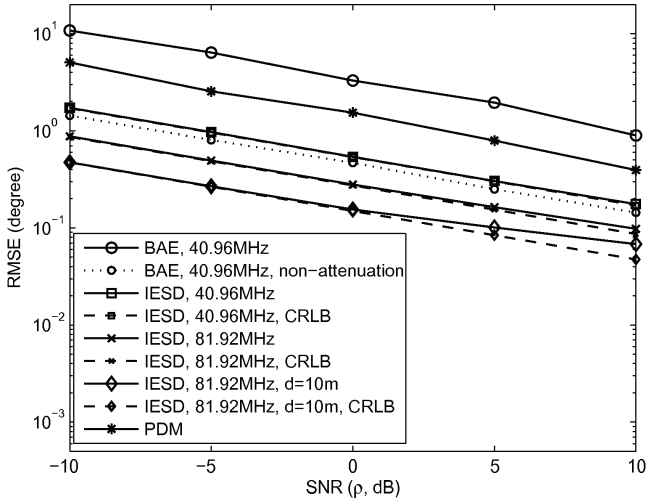

Fig. 4. RMSE performance comparison versus SNR between our methods (BAE and IESD) and PDM under scenarios with only LOS paths. Four arrays are adopted in IESD while the sweeping process is repeated four times in BAE for fairness.

B. Scenarios with Multipath Propagation

In the multipath scenarios, following the observations of [27], [29], we model the interval between the adjacent propagation paths by an exponential distribution with the mean parameter μ, i.e., the arrival statistics of the multipaths are random variables following a Poisson distribution. The magnitude of channel attenuation $\alpha_{Xi,m}$ ($X = A, B$ and $m = 1, 2, \cdots, M$) is modeled by the *Rician distribution* [25], i.e., $\alpha_{Xi,m} = \sqrt{\frac{\kappa}{\kappa+1}}\sigma_{Xi,m}e^{j\vartheta_{Xi,m}} + \sqrt{\frac{1}{\kappa+1}}\mathcal{CN}(0,\sigma_{Xi,m}^2)$ where $\mathcal{CN}(0,\sigma_{Xi,m}^2)$ denotes a circular symmetric complex Gaus-

[4]In the non-attenuation environment, IESD with four arrays is equivalent to BAE with four periods.

[5]The maximum d under the configuration in this example is 14.6 m from (10).

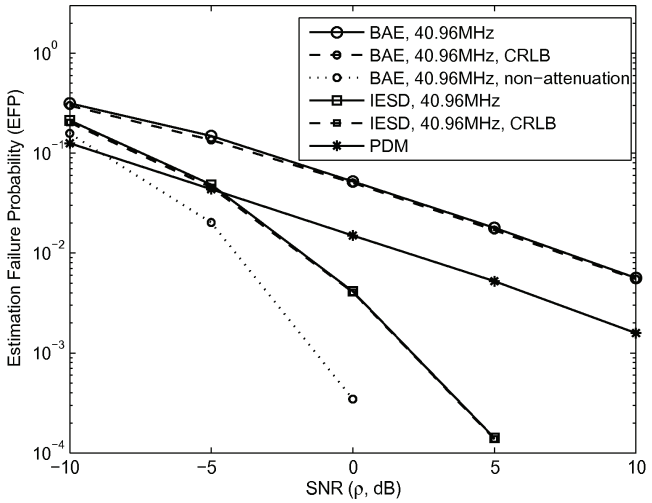

Fig. 5. EFP performance comparison versus SNR between our methods (BAE and IESD) and PDM under scenarios with only LOS paths. Four arrays are adopted in IESD while the sweeping processing is repeated four times in BAE for fairness.

sian random variable with variance $\sigma^2_{Xi,m}$, and $\vartheta_{Xi,m}$ obeys uniform distribution from 0 to 2π. The parameter κ represents the deterministic degree of the channel attenuation. Assume the power delay profile follows the classical exponential decay model [27], [28] $E\{|\alpha_{Xi,m}|^2\} = \sigma^2_{Xi,m} = \mathrm{e}^{-(\tau_{Xi,m}-\tau_{X1,m})/\Gamma}$ with $\Gamma = 50$ ns being the decay time constant. We set SNR=0 dB, $d = 10$ m, $\beta = 0.8\,\mathrm{MHz}/1$ ms, and $K = 16$, and thus the sweep bandwidth is 81.92 MHz.

In the following, we investigate the distribution of the absolute angle estimation error to evaluate the estimation performance. In the simulations, the sensor nodes are randomly distributed in the sector area with AOD from $\pi/6$ to $5\pi/6$ and distance from 20 m to 200 m between the anchor. The number of multipaths between the transceivers is P=Q=9. Although the total number of frequency components around SFO is up to $P\times Q = 81$, we set $L_p = 4$ in the simulations unless otherwise specified, which is verified to be large enough to capture all the considerable components and no noticeable performance improvement is obtained by a larger L_p. For comparison, we consider another distributed angle estimation system referred to as 'ULA-AOA', where each sensor is equipped with one uniform linear array (ULA) with M_r antenna elements and antenna spacing of half wavelength. Let the sensors estimate AOA of the wave from an anchor using the ML method in [7] with a total of MKN snapshots. Assume the channels in this system follow the same configuration as ours. Moreover, we assume the incidence angles of the reflection paths at the receiving ULA are randomly distributed in all directions after bouncing from the surrounding scatterers [25]. Note that we will not include the results of PDM due to its much worse performance under multipath channels. The following results are obtained from 10^4 independent trials.

Fig. 6 illustrates the cumulative distribution function (CDF) comparison of the absolute angle estimation error between BAE and ULA-AOA. In this example, we assume the channel attenuations are all completely deterministic, i.e., $\kappa = \infty$. Only two iterations, i.e., $L_c = 2$, are verified enough to guarantee convergence and no significant improvement can be obtained with additional iterations. We make the following observations. The results demonstrate that, statistically, the multipaths will be distributed more sparsely with a larger parameter μ, thus leading to the performance improvement. On the other hand, we also show the performance with $L_c = 0$, i.e., with no iteration, by the dashed curves. As compared with the original iterative algorithm, there indeed exists some performance degradation from the simulation results. However, for some scenarios where sensor nodes are hard to afford the computational complexity of the iterative process, this simplified approach may be more acceptable. Moreover, the results show that with more antennas, ULA-AOA could work better than BAE under some scenarios. However, we should emphasize that ULA-AOA needs one MAS at each sensor which increases the hardware cost for sensor nodes, whereas this is not required in our methods. Note that [7] would also work if the sensors are emitters and only the anchor is equipped with ULA. Similar to [10], the anchor can estimate AOA and then feed back to the sensors. However, as we have discussed earlier, this approach is not completely distributed.

Next, we investigate the performance in completely non-deterministic channels, i.e., $\kappa = 0$. The CDF comparison of the absolute estimation error between our methods (BAE and IESD) and ULA-AOA is shown in Fig. 7, where $\mu = 100$ ns is assumed in this example. The results clearly demonstrate the superiority of IESD. It can be observed that, in BAE, there exists slight performance improvement when additional periods are transmitted because the signals in these periods experience the same multipath channel. However, in IESD where multiple periods are transmitted by multiple arrays, the exploited multipath channel diversity could significantly improve the performance. Moreover, we see that although ULA-AOA behaves better than BAE, it still suffers from much higher occurrence of large estimation errors than IESD, even with $M_r = 16$ antennas adopted at each sensor. Again, we should note that our methods do not rely on MAS at each sensor, which is a significant advantage especially in large scale networks. On the other hand, bearing in mind that PDM relies on pure sinusoids and ULA-AOA works with narrowband signals, it is fair to say that we obtain these benefits at the price of using linear chirp waves.

VI. Conclusions

We have investigated a new distributed angle estimation method for WSNs in multipath propagation environment. A two-antenna anchor is employed to emit two linear chirp waves with slight frequency difference and produce an interference field. Then, AOD of the emitted waves is estimated at each receiving single-antenna sensor via frequency measurement of the local RSSI signal. Furthermore, an improved method, which exploits the space diversity from multiple parallel arrays at the anchor, has been proposed. Both the performance analysis and simulations have been presented. The proposed methods deployed in real testbeds are left as our future work.

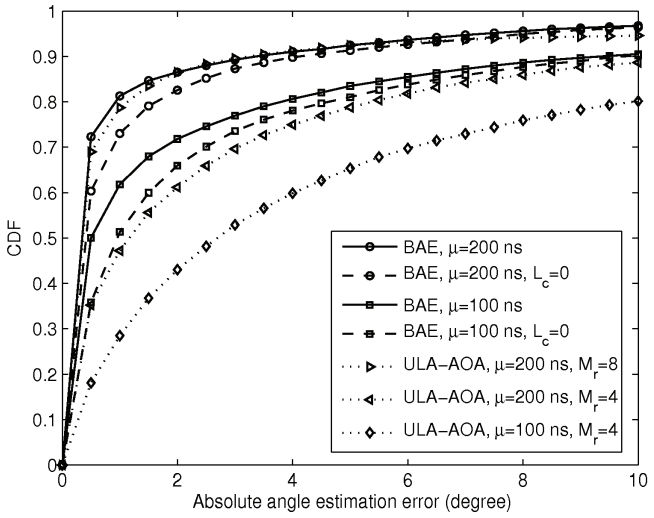

Fig. 6. CDF comparison of the absolute angle estimation error between BAE and ULA-AOA with completely deterministic channels.

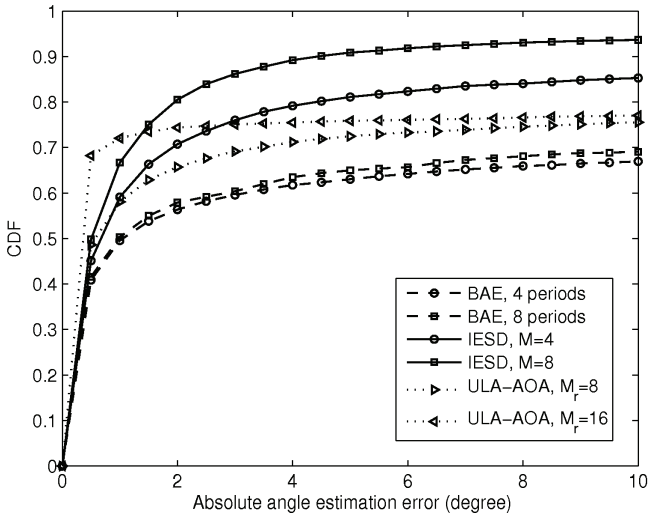

Fig. 7. CDF comparison of the absolute angle estimation error between our methods (BAE and IESD) and ULA-AOA with nondeterministic channels.

REFERENCES

[1] I. F. Akyildiz, W. Su, Y. Sankarasubramaniam, and E. Cayirci, "A survey on sensor networks," *IEEE Commun. Mag.*, vol. 40, no. 8, pp. 102–114, Aug. 2002.

[2] S. F. A. Shah and A. H. Tewfik, "Performance analysis of directional beacon based position location algorithm for UWB systems," in *Proc. 2005 IEEE GLOBECOM*, vol. 4, pp. 2409–2413.

[3] A. Nasipuri and K. Li, "A directionality based location discovery scheme for wireless sensor networks," in *Proc. 2002 ACM Workshop on Wireless Sensor Networks and Applications*, pp. 105–111.

[4] S. F. A. Shah, S. Srirangarajan, and A. H. Tewfik, "Implementation of a directional beacon-based position location algorithm in a signal processing framework," *IEEE Trans. Wireless Commun.*, vol. 9, no. 3, pp. 1044–1053, Mar. 2010.

[5] S. E. Lipsky, *Microwave Passive Direction Finding*. Wiley Interscience, 1987.

[6] A. V. Alejos, M. G. Sanchez, D. R. Iglesias, and I. Cuiñas, "Incidence angle estimation algorithm for a low-cost AoA based indoor location system," in *Proc. 2009 IEEE Int. Sym. Antennas and Propagation*, pp. 1–4.

[7] I. Ziskind and M. Wax, "Maximum likelihood localization of multiple sources by alternating projection," *IEEE Trans. Acoustics, Speech, and Signal Processing*, vol. 36, no. 10, pp. 1553–1560, Oct. 1988.

[8] H. D. Griffiths, "New ideas in FM radar," *Electronics and Commun. Engineering*, vol. 2, no. 5, pp. 185–194, Oct. 1990.

[9] D. Niculescu and B. Nath, "Ad hoc positioning system (APS) using AOA," in *Proc. 2003 INFOCOM*, vol. 3, pp. 1734–1743.

[10] Z Shan and T.-S. P. Yum, "Precise localization with smart antennas in ad-hoc networks," in *Proc. 2007 IEEE GLOBECOM*, pp. 1053–1057.

[11] W. Wang, W. Zhang, and Q. Yin, "A distributive localization method for wireless sensor networks using angle of departure," *J. Xi'an Jiaotong Univ.*, vol. 44, no. 2, pp. 61–66, Feb. 2010.

[12] I. Amundson, J. Sallai, X. Koutsoukos, and A. Ledeczi, "Radio interferometric angle of arrival estimation," in *Proc. 2010 European Conference on Wireless Sensor Networks (EWSN)*, pp. 1–16.

[13] B. H. Fleury, M. Tschudin, R. Heddergou, D. Dahlhaus, and K. I. Pedersen, "Channel parametrers estimation in mobile radio environments using SAGE algorithm," *IEEE J. Sel. Areas Commun.*, vol. 17, no. 3, pp. 434–449, Mar. 1999.

[14] H. C. So, K. W. Chan, Y. T. Chan, and K. C. Ho, "Linear prediction approach for efficient frequency estimation of multiple real sinusoids: algorithms and analyses," *IEEE Trans. Signal Process.*, vol. 53, no. 7, pp. 2290–2305, July 2005.

[15] X. Li and K. Pahlavan, "Super-resolution TOA estimaiton with diversity for indoor geolocation," *IEEE Trans. Wireless Commun.*, vol. 3, no. 224–234, pp. 224–234, Jan. 2004.

[16] R. Roy and T. Kailath, "ESPRIT-estimation of signal parameters via rotational invariance techniques," *IEEE Trans. Acoust. Speech, Signal Process.*, vol. 37, no. 7, pp. 984–995, July 1989.

[17] H. Xu, C.-C. Chong, I. Guvenc, F. Watanabe, and L. Yang, "High-resolution TOA estimation with multi-band OFDM UWB signals," in *Proc. 2008 IEEE ICC*, pp. 4191–4196.

[18] M. Feder and E. Weinstein, "Parameter estimation of superimposed signals using the EM algorithm," *IEEE Trans. Acoust., Speech, Signal Process.*, vol. 36, no. 4, pp. 477–682, Apr. 1988.

[19] F. Gao and A. Nallanathan, "Blind maximum likelihood CFO estimation for OFDM systems via polynomial rooting," *IEEE Signal Process. Lett.*, vol. 13, no. 2, pp. 73–76, Feb. 2006.

[20] C. Li and W. Zhuang, "Nonline-of-sight error mitigation in mobile location," *IEEE Trans. Wireless Commun.,* vol. 4, no. 2, pp. 560–573, Feb. 2005.

[21] P. Stoica and A. Nehorai, "MUSIC, maxixmum likelihood, and Cramer-Rao Bound," *IEEE Trans. Acoustics, Speech, and Signal Process.*, vol. 37, no. 5, pp. 720–741, May 1989.

[22] W. Xiao and Y. Peng, "Two fast ESPRIT algorithms," *ACTA Electronica Sinica*, vol. 23, no. 7, pp. 102–104, July 1995.

[23] I. S. Gradshteyn and I. M. Ryzhik, *Table of Integrals, Series, and Products*, 7th edition. Academic Press of Elsevier, 2007.

[24] G. H. Golub and C. F. V. Loan, *Matrix Computations*. Johns Hopkins University Press, 1996.

[25] D. Tse, *Fundamentals of Wireless Communication*. Cambridge University Press, 2004.

[26] A. Boukerche, H. A. B. Oliveira, E. F. Nakamura, and A. A. F. Loureiro, "Localization systems for wireless sensor networks," *IEEE Wireless Commun.*, vol. 14, no. 6, pp. 6–12, Dec. 2007.

[27] A. A. M. Saleh and R. A. Valenzuela, "A statistical model for indoor multipath propagation," *IEEE J. Sel. Areas Commun.*, vol. 5, no. 2, pp. 128–137, Feb. 1987.

[28] A. F. Molisch, "Ultra-wide-band propagation channels," *Proc. IEEE*, vol. 97, no. 2, pp. 1528–1545, Sep. 2009.

[29] G. L. Turin, F. D. Clapp, T. L. Johnston, S. B. Fine, and D. Lavry, "A statistical model of urban multipath propagation," *IEEE Trans. Veh. Technol.*, vol. 21, no. 1, pp. 1–9, Feb. 1972.

Weile Zhang received the Ph.D degree in Information and Communication Engineering from Xi'an Jiaotong University, Xi'an, China, in 2012. From October 2010 to October 2011, he was a visiting scholar at the Department of Computer Science, University of California, Santa Barbara, CA, USA. His research interests include broadband wireless communications, array signal processing and localization in wireless networks.

Qinye Yin received the B.S., M.S., and Ph.D. degrees in Communication and Electronic Systems from Xi'an Jiaotong University, Xi'an, China, in 1982, 1985, and 1989, respectively. Since 1989, he has been on the faculty at Xi'an Jiaotong University, where he is currently a Professor of Information and Communications Engineering Department and Chair of Academy Committee of School of Electronic and Information Engineering. From 1987 to 1989, he was a visiting scholar at the University of Maryland, MD, USA. From June to December 1996, he was a visiting scholar at the University of Taxes, Austin, TX, USA. His research interests focus on the joint time-frequency analysis and synthesis, the theory and applications of wireless sensor networks, multiple antenna MIMO broadband communication systems (including smart antenna systems), parameter estimation, and array signal processing.

Hongyang Chen was born in China. He received the Ph.D degree from the Univ. of Tokyo. In 2009, he was a visiting researcher in the UCLA Adaptive Systems Laboratory at University of California Los Angeles. His research interests include Wireless Sensor Networks, Signal Processing for Communications.

Feifei Gao (S'05-M'09) received the B.Eng. degree from Xi'an Jiaotong University, Xi'an, China in 2002, the M.Sc. degree from McMaster University, Hamilton, ON, Canada, in 2004, and the Ph.D degree from National University of Singapore, Singapore, in 2007.

He was a Research Fellow with the Institute for Infocomm Research, A*STAR, Singapore, in 2008 and an Assistant Professor with the School of Engineering and Science, Jacobs University, Bremen, Germany, from 2009 to 2010. In 2011, he joined the Department of Automation, Tsinghua University, Beijing, China, where he is currently an Associate Professor. He also serves as an Adjunct Professor with the School of Engineering and Science, Jacobs University. He has coauthored more than 90 refereed IEEE journal and conference proceeding papers. His research interests are communication theory, broadband wireless communications, signal processing, multiple-input-multiple-output systems, and array signal processing.

Prof. Gao has served on the Editorial Board of IEEE WIRELESS COMMUNICATIONS LETTERS, and as a Technical Program Committee member for the IEEE International Conference on Communications, the IEEE Global Communications Conference, the IEEE Vehicular Technology Conference, and the IEEE Personal, Indoor, and Mobile Radio Communications Conference.

Nirwan Ansari (S'78-M'83-SM'94-F'09) received the B.S.E.E. (summa cum laude with a perfect GPA) from the New Jersey Institute of Technology (NJIT), Newark, in 1982, the M.S.E.E. degree from University of Michigan, Ann Arbor, in 1983, and the Ph.D degree from Purdue University, West Lafayette, IN, in 1988. He joined NJIT's Department of Electrical and Computer Engineering as Assistant Professor in 1988, became a tenured Associate Professor in 1993, and has been a Full Professor since 1997. He has also assumed various administrative positions at NJIT. He was Visiting (Chair) Professor at several universities. He authored Computational Intelligence for Optimization (Springer, 1997) with E.S.H. Hou and edited Neural Networks in Telecommunications (Springer, 1994) with B. Yuhas. He has contributed over 400 technical papers, over one third of which were published in widely cited refereed journals/magazines. He has also guest-edited a number of special issues, covering various emerging topics in communications and networking. His current research focuses on various aspects of broadband networks and multimedia communications.

Prof. Ansari has served on the Editorial Board and Advisory Board of eight journals, including as a Senior Technical Editor of the IEEE Communications Magazine (2006-2009). He has served the IEEE in various capacities such as Chair of the IEEE North Jersey Communications Society (COMSOC) Chapter, Chair of the IEEE North Jersey Section, Member of the IEEE Region 1 Board of Governors, Chair of the IEEE COMSOC Networking Technical Committee Cluster, Chair of the IEEE COMSOC Technical Committee on Ad Hoc and Sensor Networks, and Chair/Technical Program Committee Chair of numerous conferences/symposia. Some of his recent recognitions include a 2007 IEEE Leadership Award from the Central Jersey/Princeton Section, NJIT Excellence in Teaching in Outstanding Professional Development in 2008, a 2008 IEEE MGA Leadership Award, the 2009 NCE Excellence in Teaching Award, a couple of best paper awards (IC-NIDC 2009 and IEEE GLOBECOM 2010), a 2010 Thomas Alva Edison Patent Award, and designation as an IEEE Communications Society Distinguished Lecturer (2006-2009, two terms). He was also granted over fifteen US patents.